Supporting Information

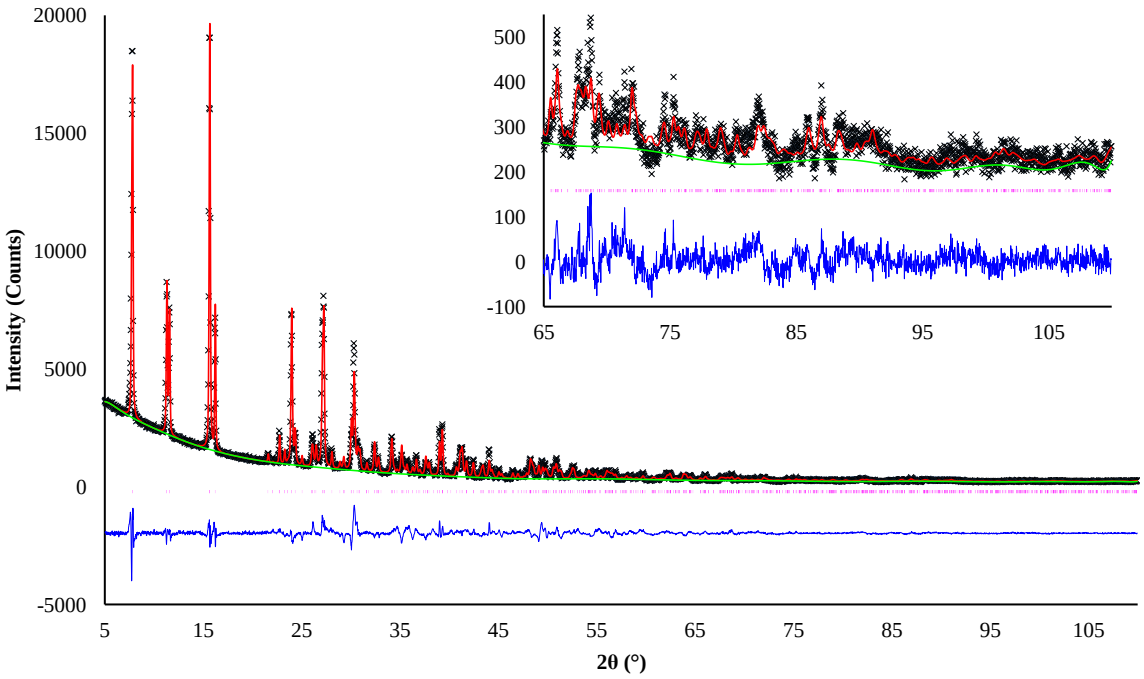

Figure S1. A plot of the Rietveld refinement of $[CuCl_2(INAm)_2]$ (**2**). Black crosses represent observed data, the red line calculated data, the green line background, the pink markers peak positions, and the blue line is the difference plot $[(I_{obs} - I_{calc})]$. The inset shows the portion of data between 65 and 110° 2θ.

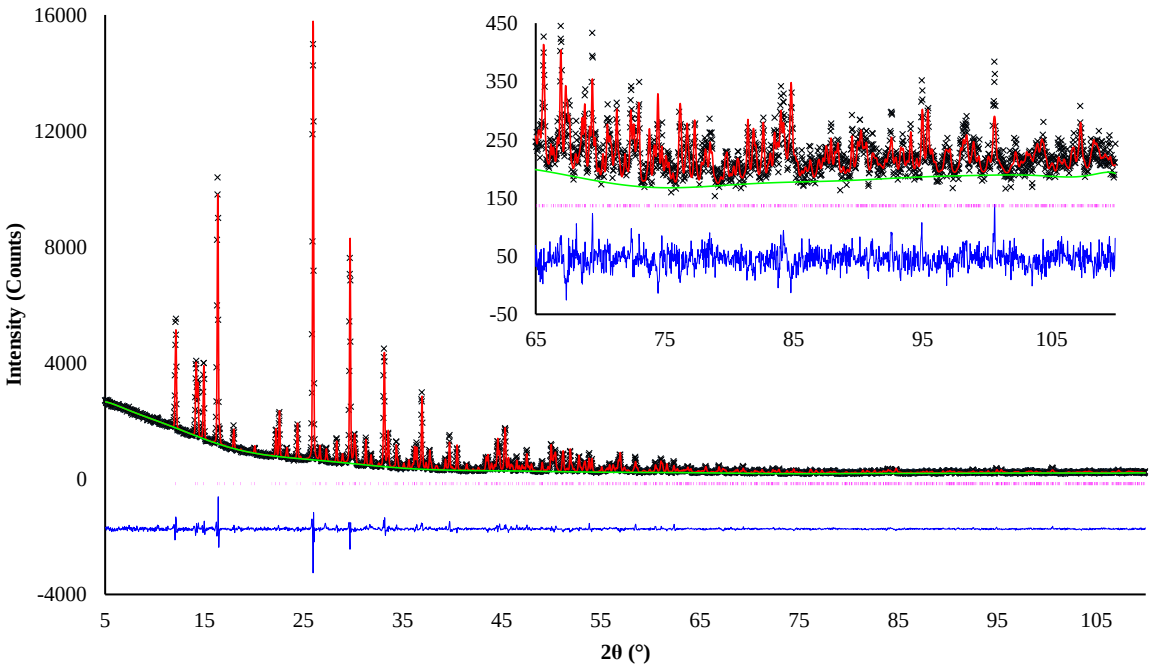

Figure S2. A plot of the Rietveld refinement of $[CuCl_4](H\text{-}INAc)_2$ (**4b**). Black crosses represent observed data, the red line calculated data, the green line background, the pink markers peak positions, and the blue line is the difference plot [($I_{obs} - I_{calc}$)]. The inset shows the portion of data between 65 and 110° 2θ.

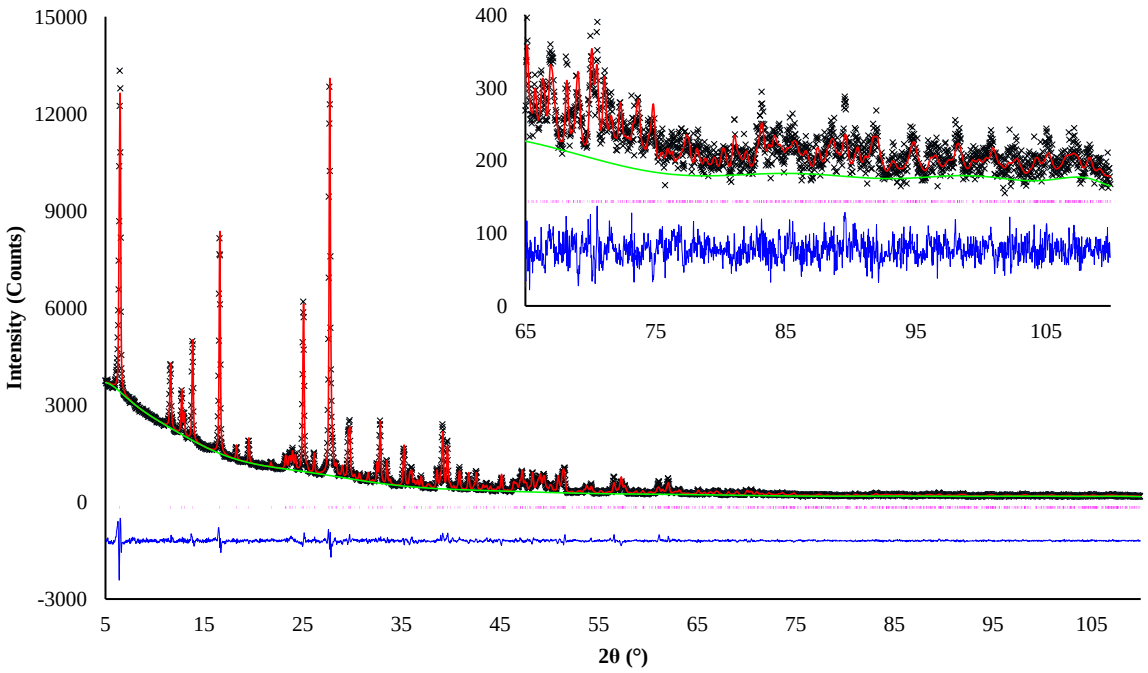

Figure S3. A plot of the Rietveld refinement of $[CuCl_4](H\text{-}INAm)_2$ (II) (**5b**). Black crosses represent observed data, the red line calculated data, the green line background, the pink markers peak positions, and the blue line is the difference plot [($I_{obs} - I_{calc}$)]. The inset shows the portion of data between 65 and 110° 2θ.

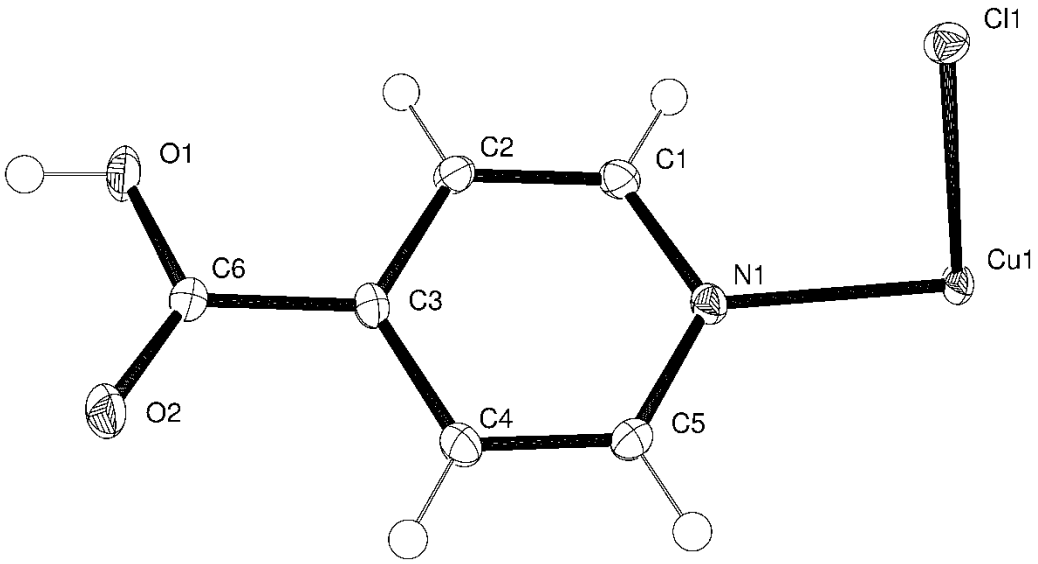

Figure S4. Asymmetric unit of **1** with atoms shown as thermal ellipsoids drawn at 50% probability.

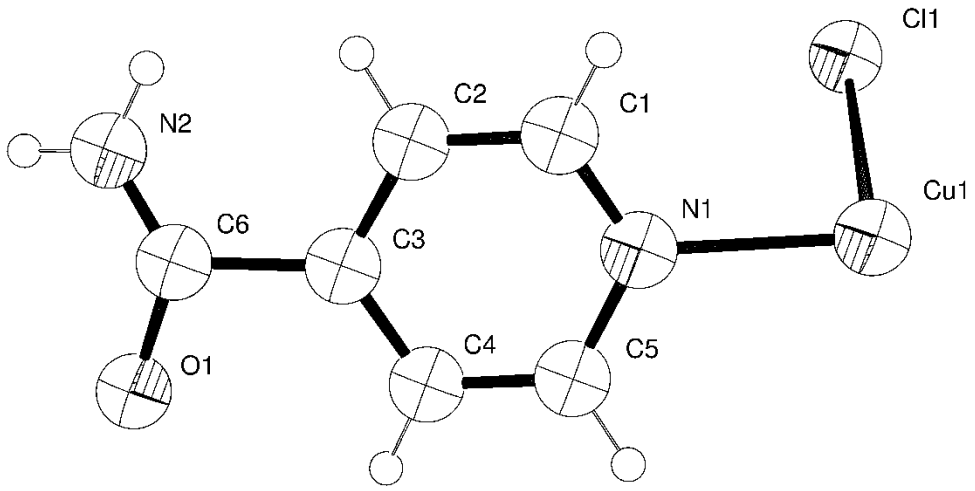

Figure S5. Asymmetric unit of **2** with atoms shown as thermal ellipsoids drawn at 50% probability.

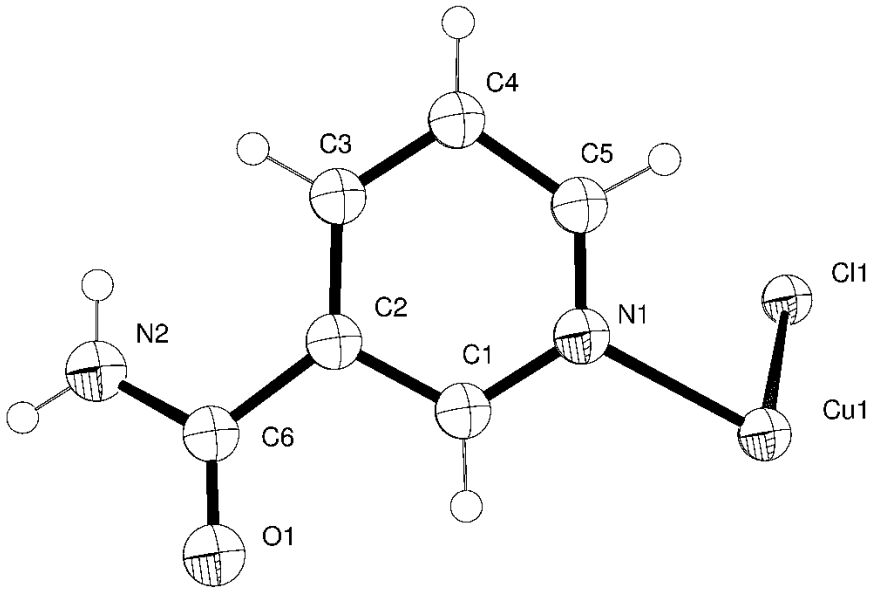

Figure S6. Asymmetric unit of **3** with atoms shown as thermal ellipsoids drawn at 50% probability.

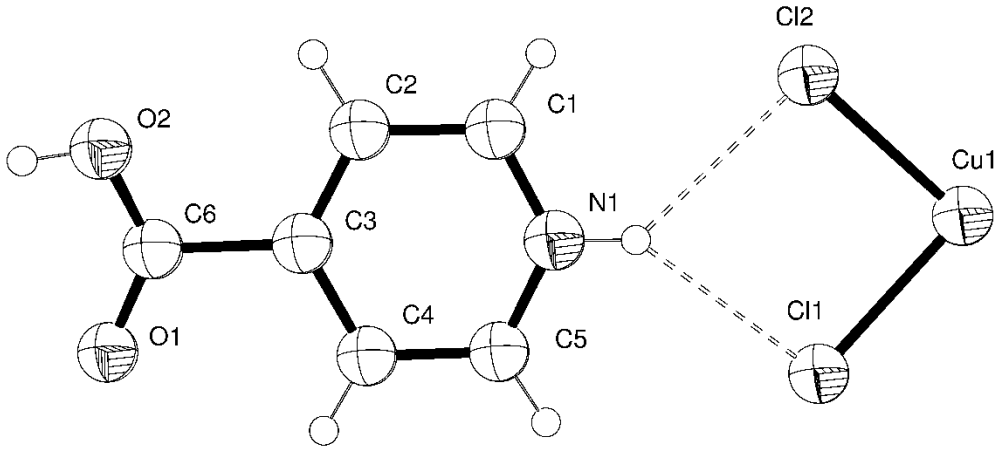

Figure S7. Asymmetric unit of **4b** with atoms shown as thermal ellipsoids drawn at 50% probability.

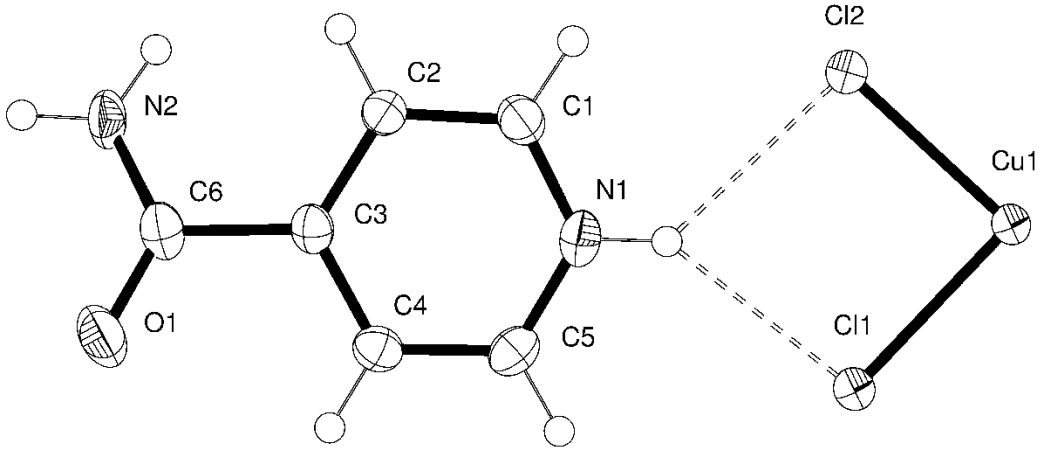

Figure S8. Asymmetric unit of **5a** with atoms shown as thermal ellipsoids drawn at 50% probability.

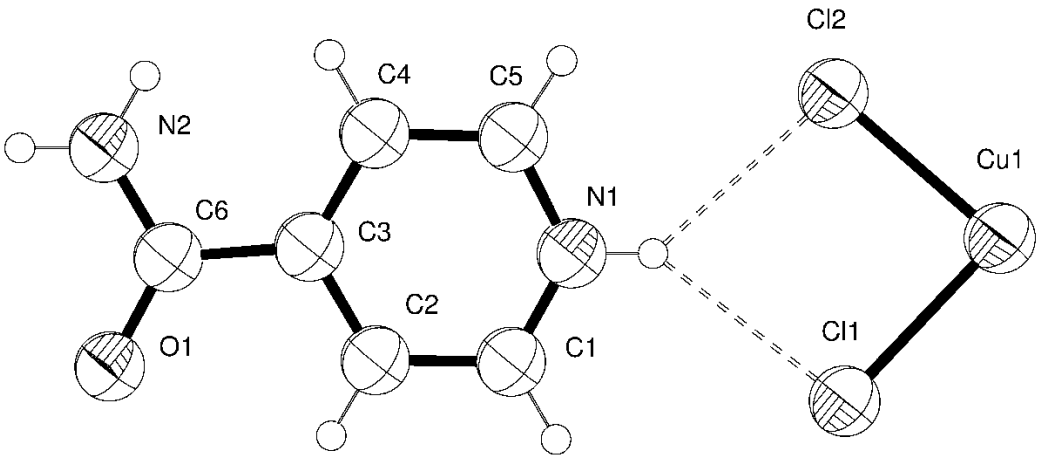

Figure S9. Asymmetric unit of **5b** with atoms shown as thermal ellipsoids drawn at 50% probability.

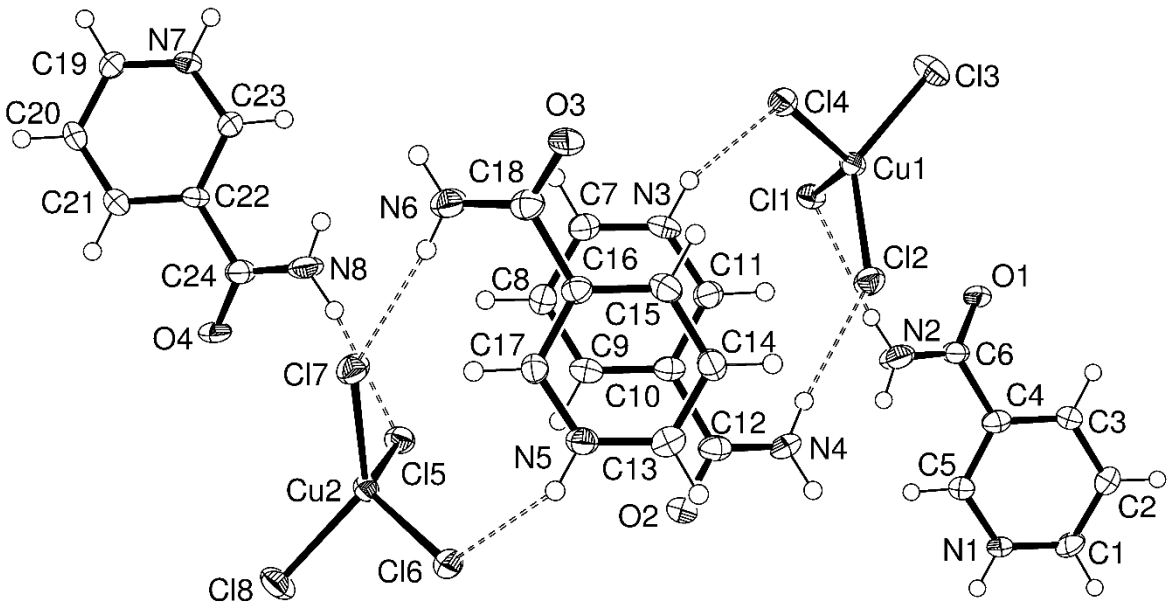

Figure S10. Asymmetric unit of **6a** with atoms shown as thermal ellipsoids drawn at 50% probability.

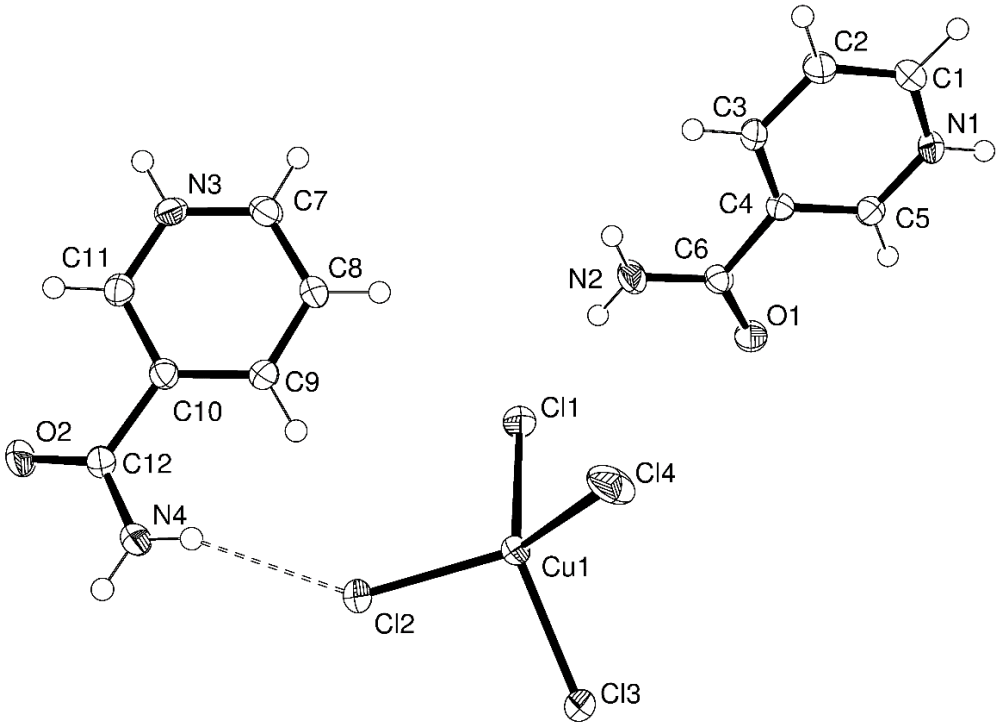

Figure S11. Asymmetric unit of **6b** with atoms shown as thermal ellipsoids drawn at 50% probability.

Table S1. Bond angles of the atoms coordinated to the Cu centre in **1**

Atoms	Bond Angle (°)
N(1)#1-Cu(1)-N(1)	180
N(1)#1-Cu(1)-Cl(1)#1	89.35(5)
N(1)-Cu(1)-Cl(1)#1	90.65(5)
N(1)#1-Cu(1)-Cl(1)	90.65(5)
N(1)-Cu(1)-Cl(1)	89.35(5)
Cl(1)#1-Cu(1)-Cl(1)	180

Symmetry transformations used to generate equivalent atoms:

#1 -x, -y+2, -z+2

Table S2. Bond angles of the atoms coordinated to the Cu centre in **2**

Atoms	Bond Angle (°)
N(1)#1-Cu(1)-N(1)	180
N(1)#1-Cu(1)-Cl(1)#1	88.6(6)
N(1)-Cu(1)-Cl(1)#1	91.4(6)
N(1)#1-Cu(1)-Cl(1)	91.4(6)
N(1)-Cu(1)-Cl(1)	88.6(6)
Cl(1)#1-Cu(1)-Cl(1)	180

Symmetry transformations used to generate equivalent atoms:

#1 2-x, 2-y, 2-z

Table S3. Bond angles of the atoms coordinated to the Cu centre in **3**

Atoms	Bond Angle (°)
N(1)#1-Cu(1)-N(1)	180
N(1)#1-Cu(1)-Cl(1)#1	89.8(3)
N(1)-Cu(1)-Cl(1)#1	90.2(3)
N(1)#1-Cu(1)-Cl(1)	90.2(3)
N(1)-Cu(1)-Cl(1)	89.8(3)
Cl(1)#1-Cu(1)-Cl(1)	180

Symmetry transformations used to generate equivalent atoms:

#1 2-x, -y, -z

#2 1+x, y, z

Table S4. Bond angles of the atoms coordinated to the Cu centre in **4b**

Atoms	Bond Angle (°)
Cl(2)#1-Cu(1)-Cl(2)	180
Cl(2)#1-Cu(1)-Cl(1)#1	90.56(12)
Cl(2)-Cu(1)-Cl(1)#1	89.44(12)
Cl(2)#1-Cu(1)-Cl(1)	89.44(12)
Cl(2)-Cu(1)-Cl(1)	90.56(12)
Cl(1)#1-Cu(1)-Cl(1)	180

Symmetry transformations used to generate equivalent atoms:

#1 -x, -y, -z

Table S5. Bond angles of the atoms coordinated to the Cu centre in **5a**

Atoms	Bond Angle (°)
Cl(2)#1-Cu(1)-Cl(2)	180
Cl(2)#1-Cu(1)-Cl(1)#1	89.60(4)
Cl(2)-Cu(1)-Cl(1)#1	90.40(4)
Cl(2)#1-Cu(1)-Cl(1)	90.40(4)
Cl(2)-Cu(1)-Cl(1)	89.60(4)
Cl(1)#1-Cu(1)-Cl(1)	180

Symmetry transformations used to generate equivalent atoms:

#1 -x+2, -y+2, -z

Table S6. Bond angles of the atoms coordinated to the Cu centre in **5b**

Atoms	Bond Angle (°)
Cl(2)#1-Cu(1)-Cl(2)	180
Cl(2)#1-Cu(1)-Cl(1)#1	88.1(2)
Cl(2)-Cu(1)-Cl(1)#1	91.9(2)
Cl(2)#1-Cu(1)-Cl(1)	91.9(2)
Cl(2)-Cu(1)-Cl(1)	88.1(2)
Cl(1)#1-Cu(1)-Cl(1)	180

Symmetry transformations used to generate equivalent atoms:

#1 -x, -y, -z

Table S7. Bond angles of the atoms coordinated to the Cu centre in **6a**

Atoms	Bond Angle (°)
Cl(3)-Cu(1)-Cl(2)	133.90(14)
Cl(3)-Cu(1)-Cl(4)	99.67(8)
Cl(2)-Cu(1)-Cl(4)	101.19(9)
Cl(3)-Cu(1)-Cl(1)	98.88(9)
Cl(2)-Cu(1)-Cl(1)	100.74(8)
Cl(4)-Cu(1)-Cl(1)	126.63(13)
Cl(8)-Cu(2)-Cl(7)	132.83(14)
Cl(8)-Cu(2)-Cl(6)	99.96(8)
Cl(7)-Cu(2)-Cl(6)	101.45(8)
Cl(8)-Cu(2)-Cl(5)	99.86(9)
Cl(7)-Cu(2)-Cl(5)	100.05(8)
Cl(6)-Cu(2)-Cl(5)	126.73(13)

Table S8. Bond angles of the atoms coordinated to the Cu centre in **6b**

Atoms	Bond Angle (°)
Cl(4)-Cu(1)-Cl(3)	98.272(19)
Cl(4)-Cu(1)-Cl(1)	98.251(18)
Cl(3)-Cu(1)-Cl(1)	135.804(17)
Cl(4)-Cu(1)-Cl(2)	137.888(19)
Cl(3)-Cu(1)-Cl(2)	96.349(16)
Cl(1)-Cu(1)-Cl(2)	98.184(18)

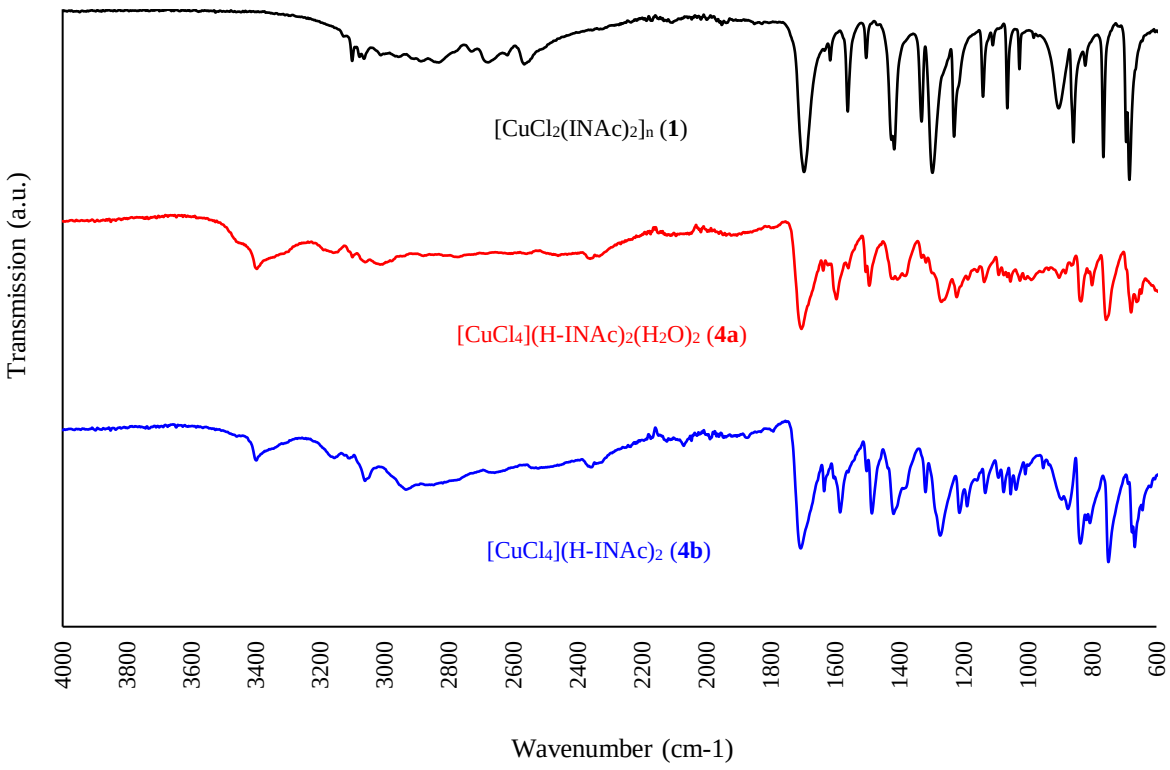

Figure S12. Infrared spectra for **1** (black), **4a**, (red) and **4b** (blue)

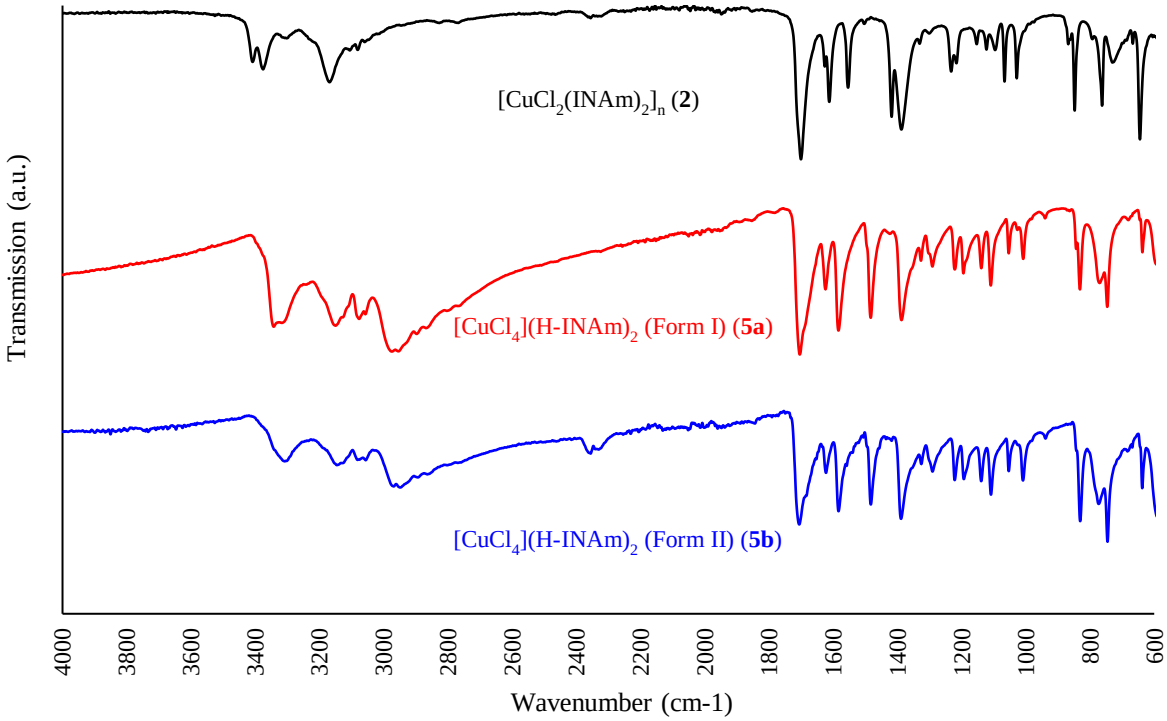

Figure S13. Infrared spectra for **2** (black), **5a**, (red) and **5b** (blue)

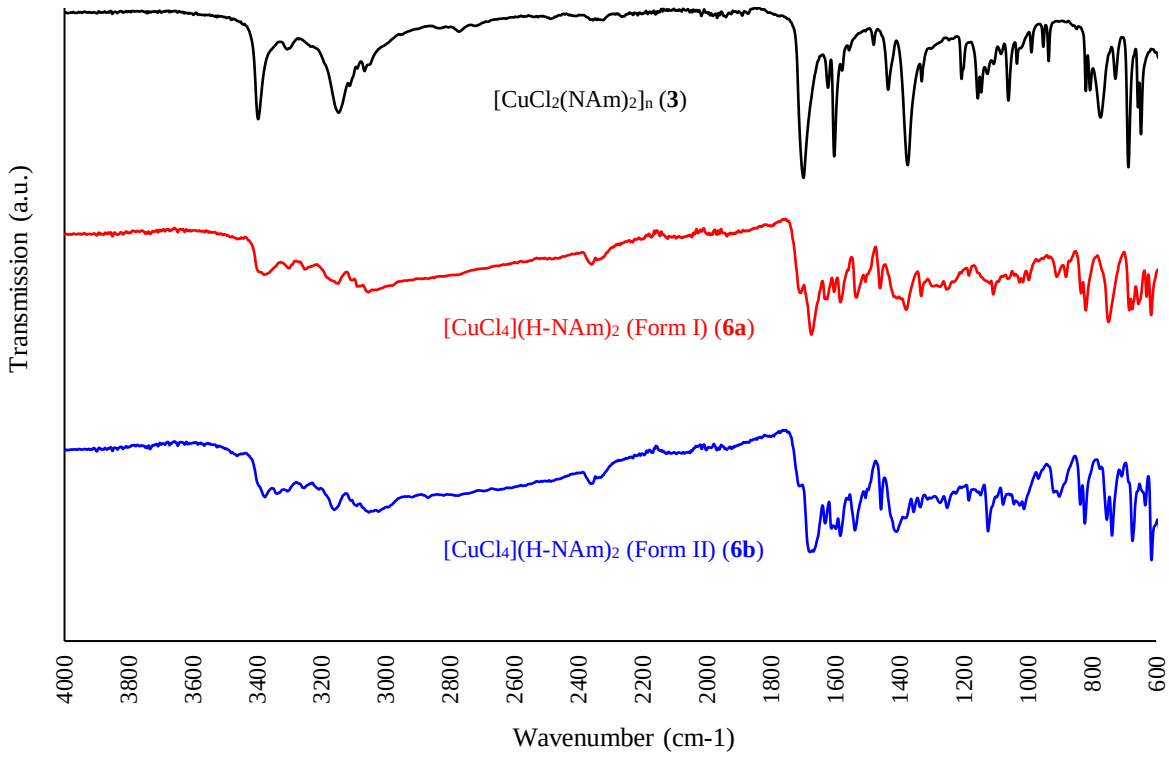

Figure S14. Infrared spectra for **3** (black), **6a**, (red) and **6b** (blue)

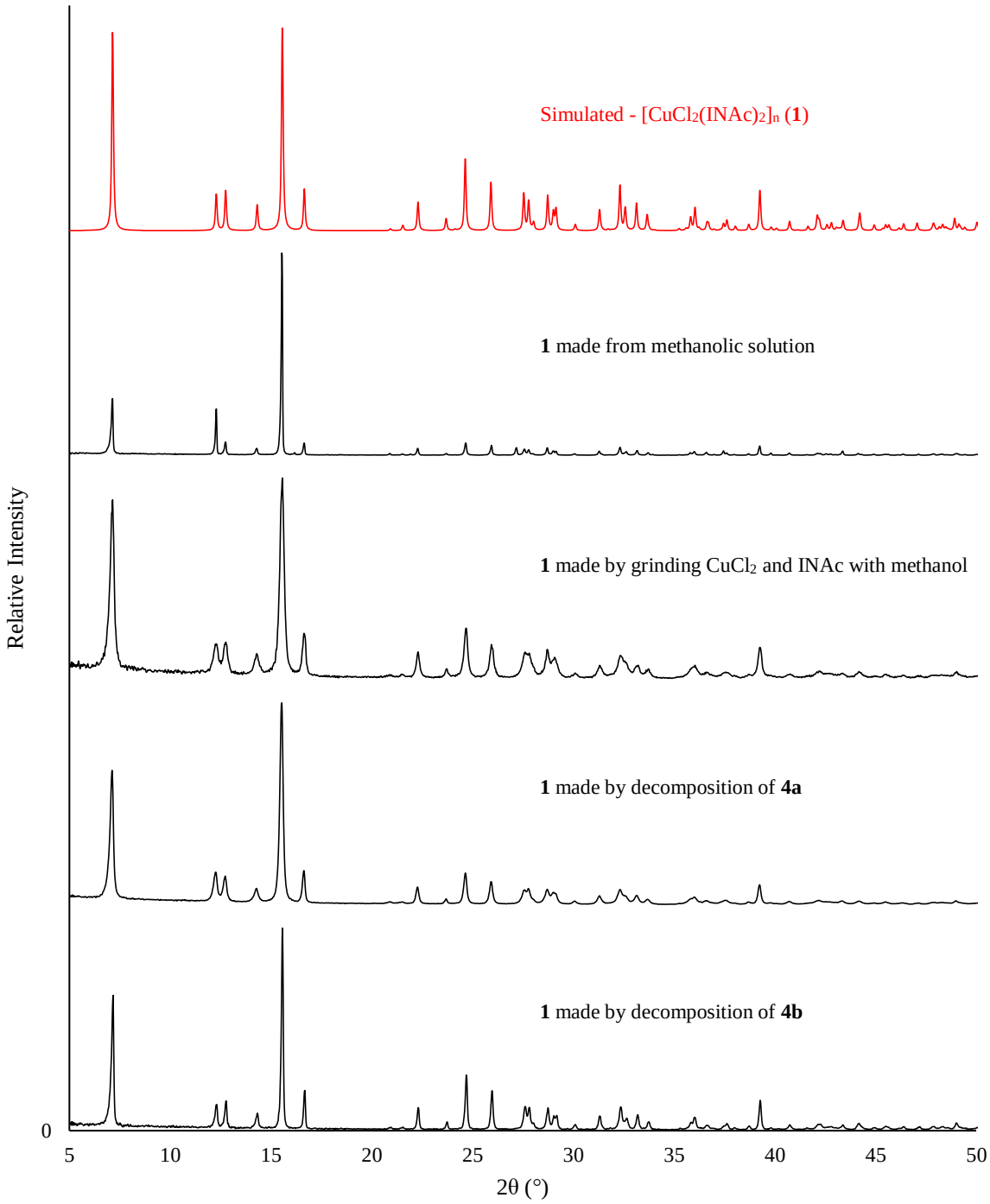

Figure S15. Room temperature X-ray powder diffraction data for samples of **1** made by solution and mechanochemical methods, and decomposition of **4a** and **4b**. Experimental data is shown in black while simulated data is shown in red.

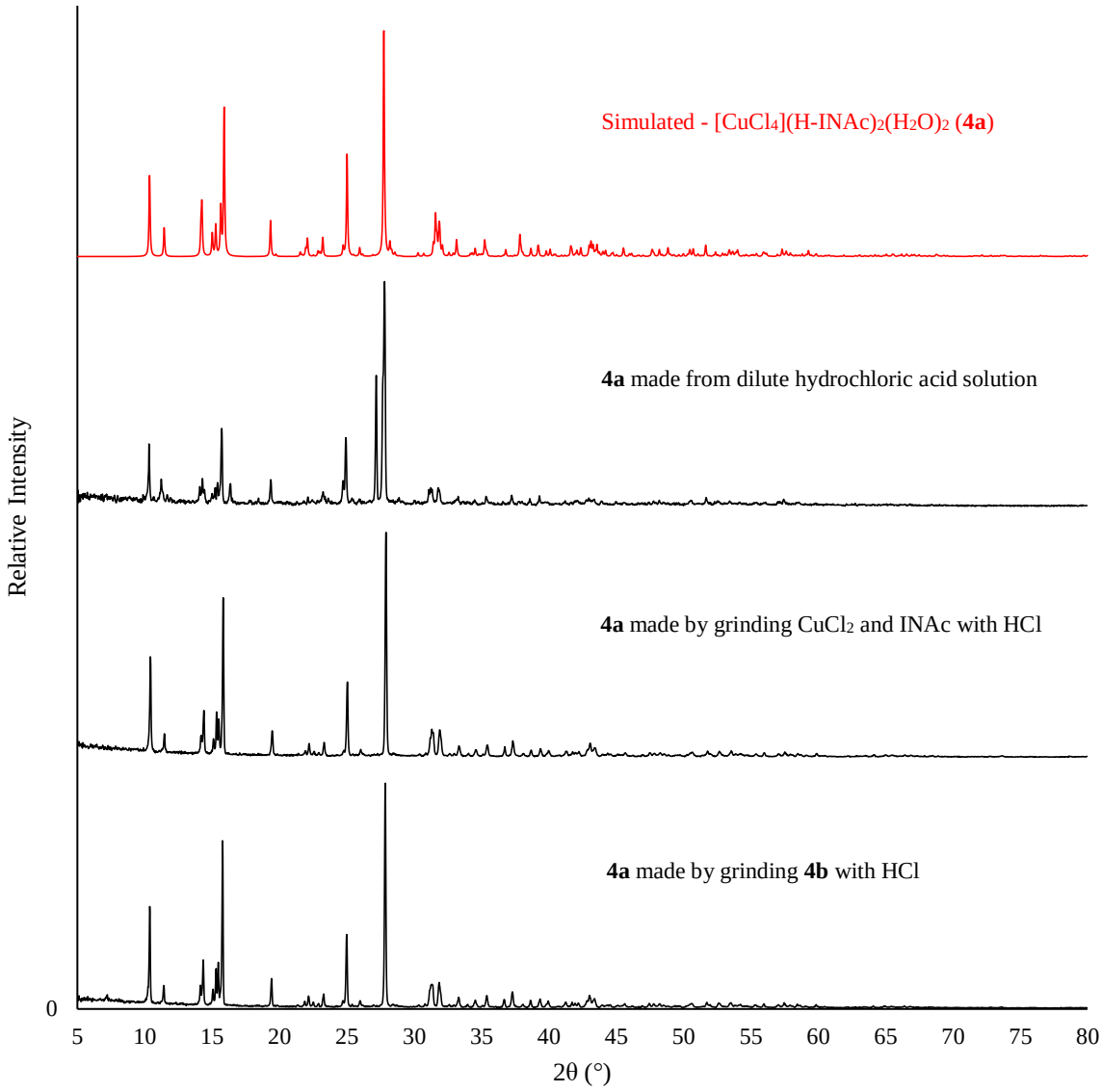

Figure S16. Room temperature X-ray powder diffraction data for samples of **4a** made using solution and mechanochemical methods. Experimental data is shown in black while simulated data is shown in red.

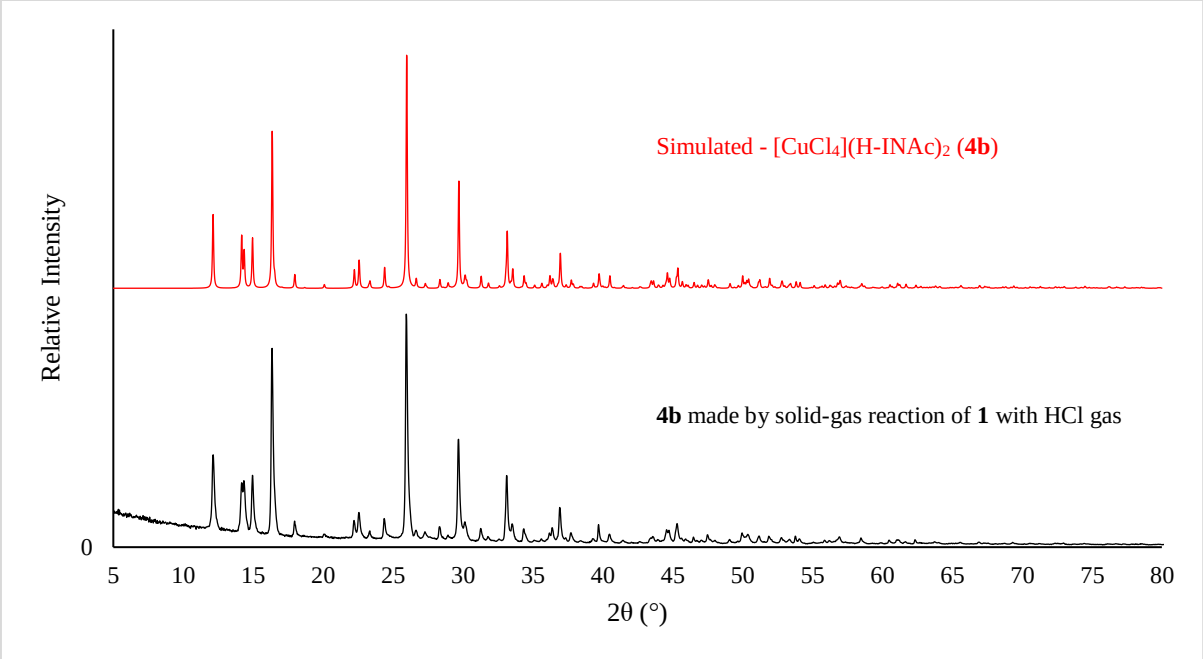

Figure S17. Room temperature X-ray powder diffraction data of **4b** made by solid-gas reaction of **1** with HCl gas. Experimental data is shown in black while simulated data is shown in red.

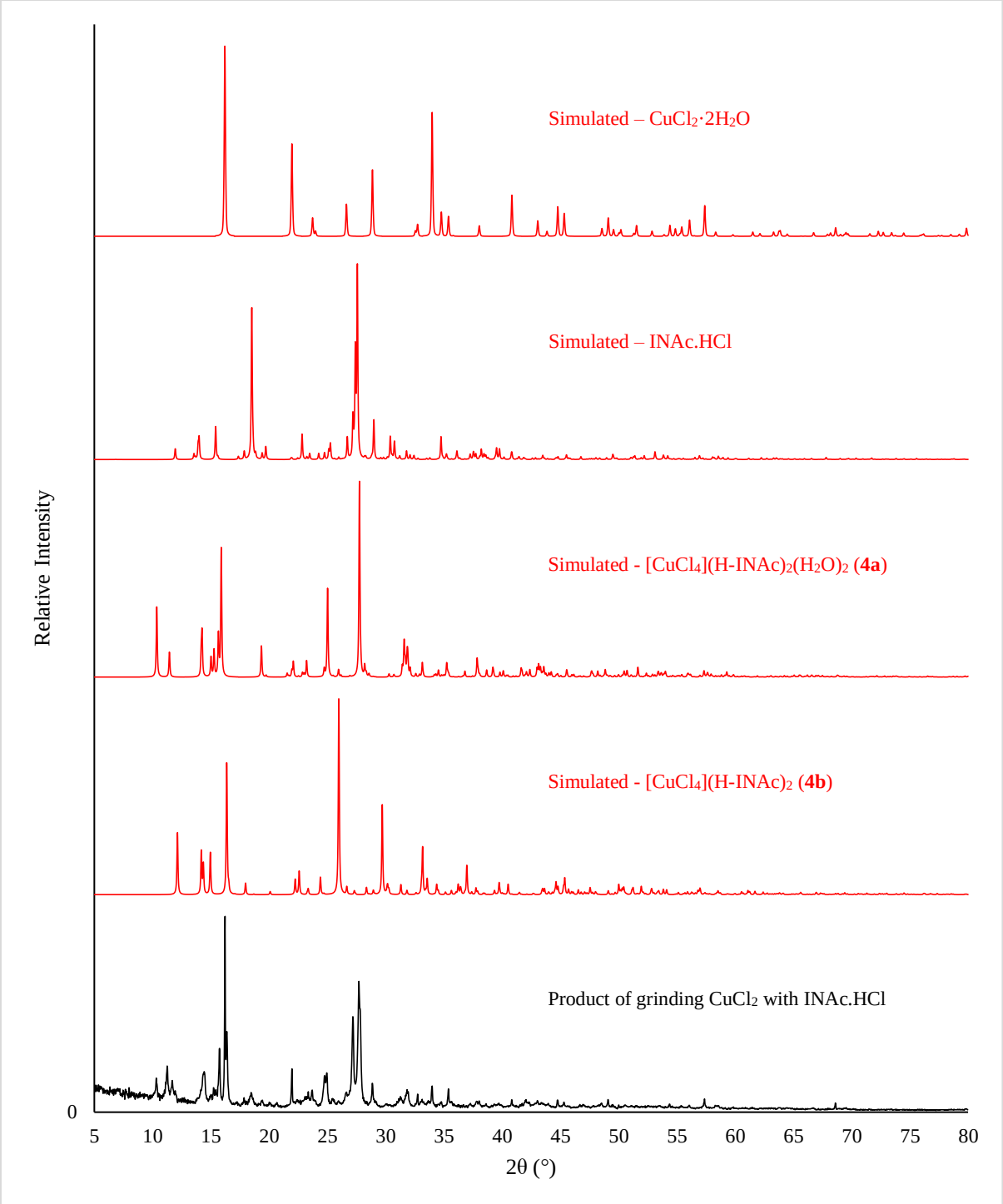

Figure S18. Room temperature X-ray powder diffraction data of the product made by mechanochemical reaction of copper chloride with INAc.HCl. Experimental data is shown in black while simulated data is shown in red.

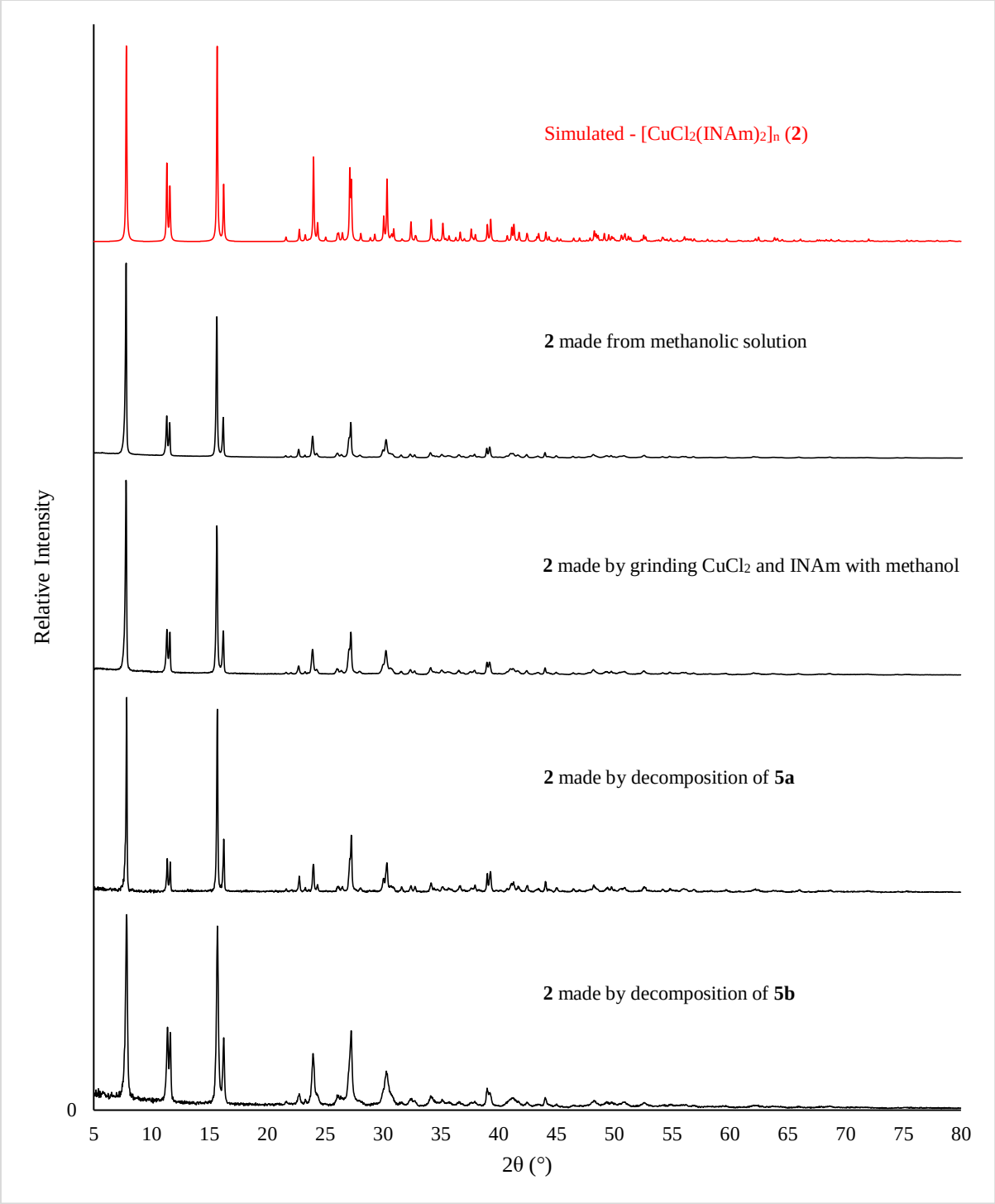

Figure S19. Room temperature X-ray powder diffraction data for samples of **2** made using solution and mechanochemical methods, and decomposition of **5a** and **5b**. Experimental data is shown in black while simulated data is shown in red.

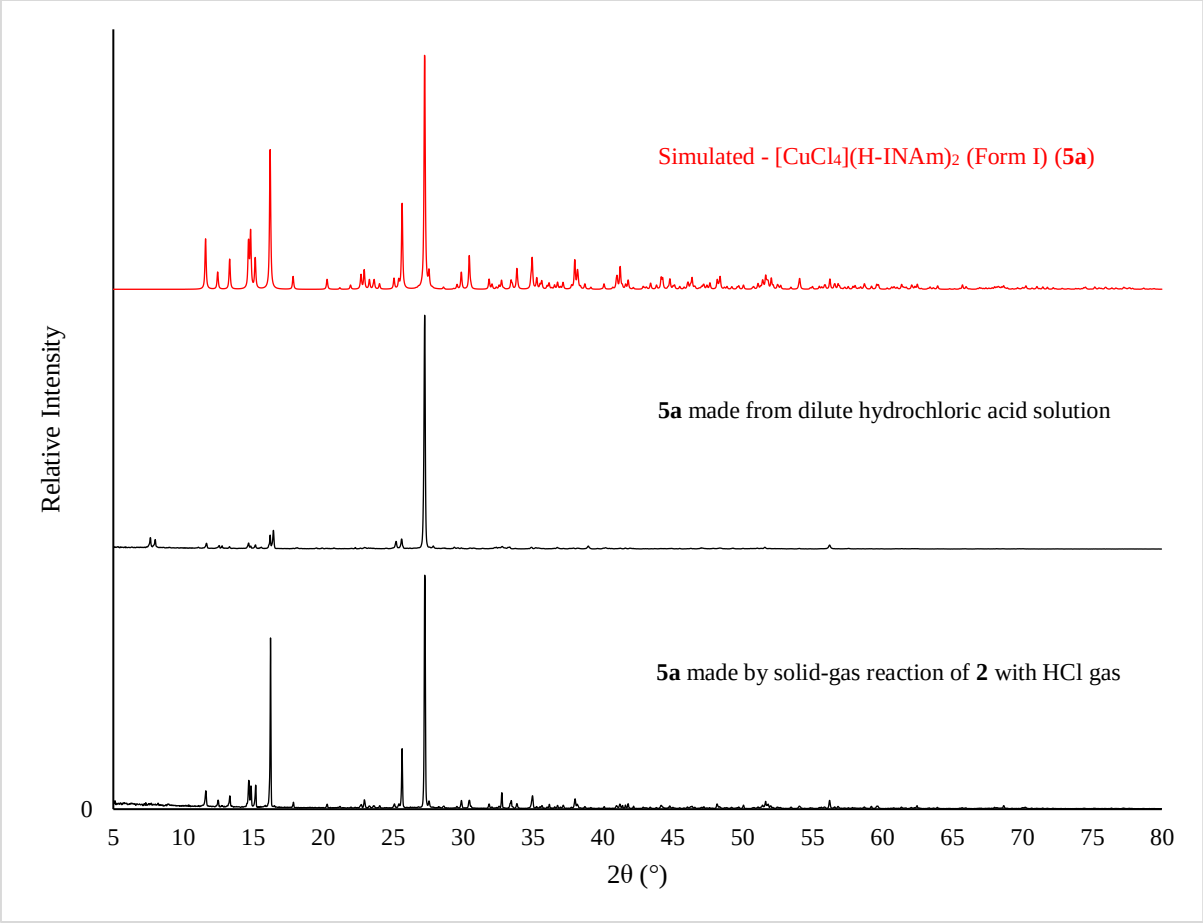

Figure S20. Room temperature X-ray powder diffraction data of **5a** made by the solution method and solid-gas reaction of **2** with HCl gas. Experimental data is shown in black while simulated data is shown in red.

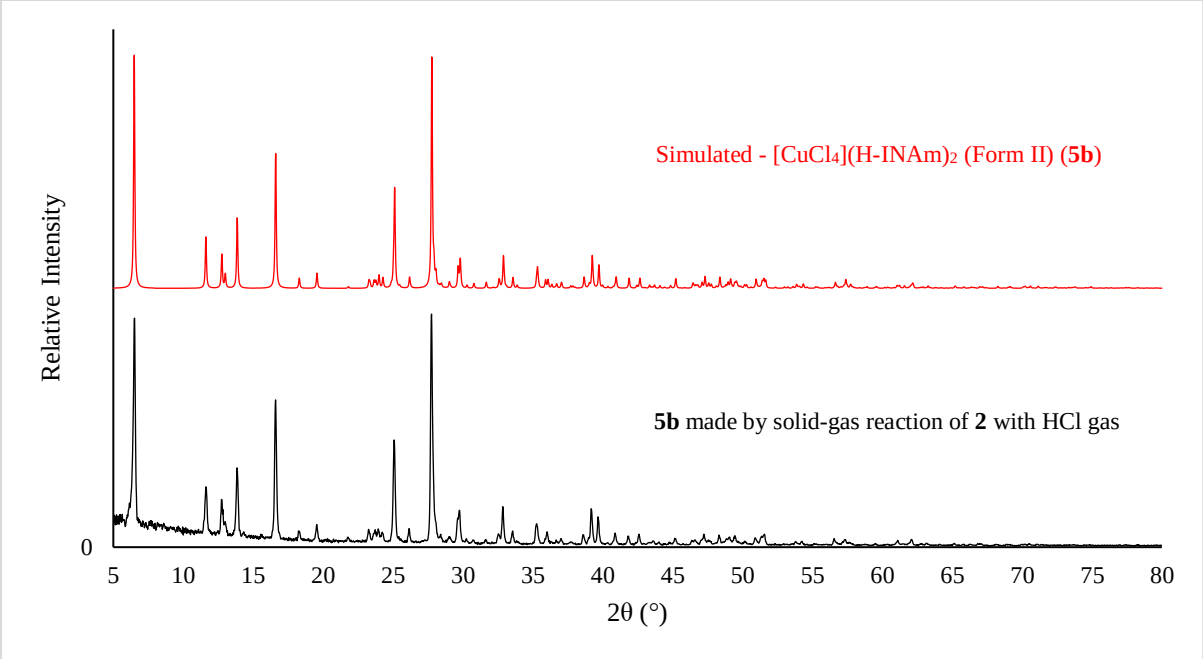

Figure S21. Room temperature X-ray powder diffraction data of **5b** made by solid-gas reaction of **2** with HCl gas. Experimental data is shown in black while simulated data is shown in red.

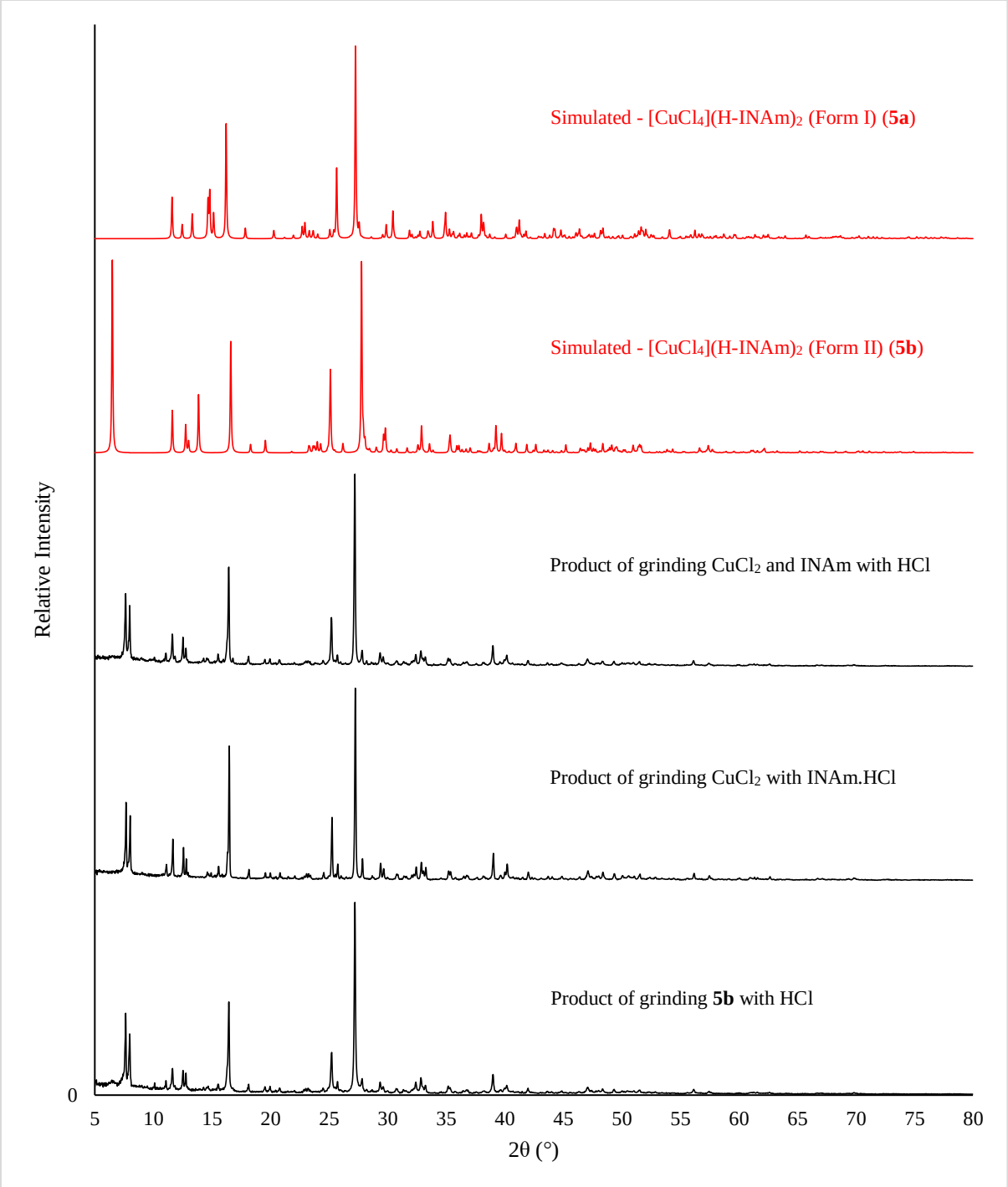

Figure S22. Room temperature X-ray powder diffraction data for samples of the products made by mechanochemical reaction of copper chloride and INAm with HCl, copper chloride and INAm.HCl and **5b** with HCl. Experimental data is shown in black while simulated data is shown in red.

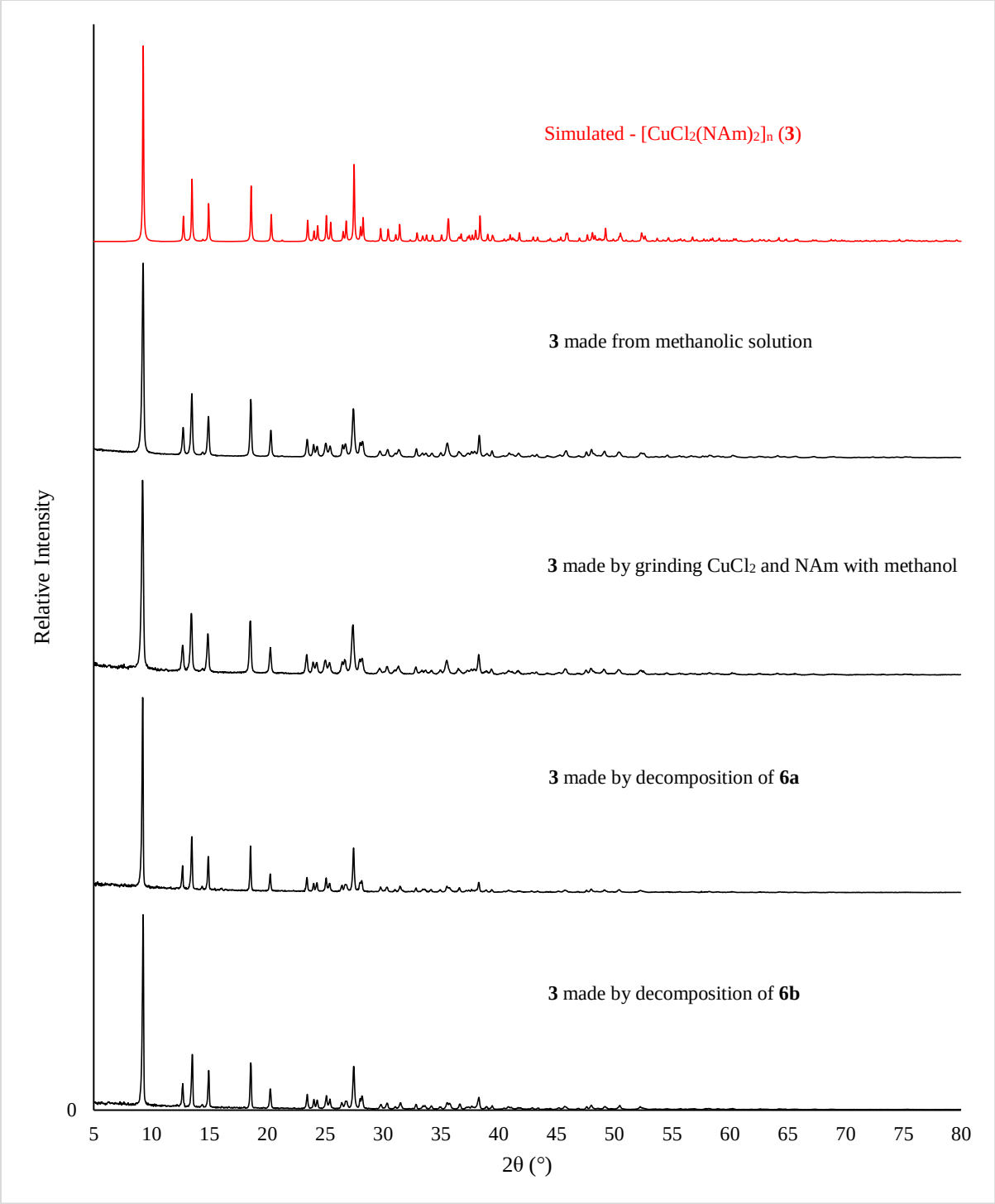

Figure S23. Room temperature X-ray powder diffraction data for samples of **3** made by solution and mechanochemical methods, and decomposition of **6a** and **6b**. Experimental data is shown in black while simulated data is shown in red.

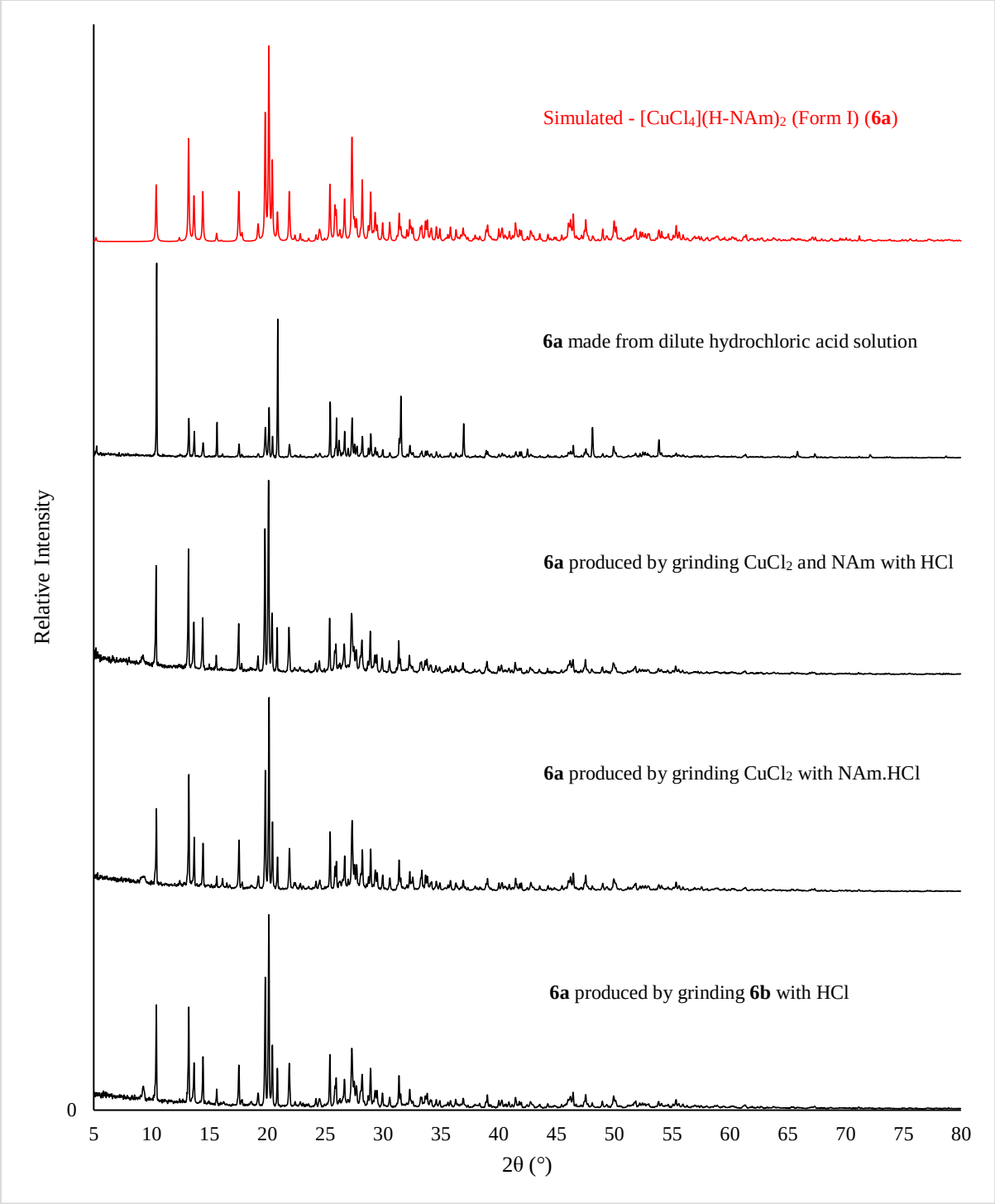

Figure S24. Room temperature X-ray powder diffraction data for samples of **6a** made by solution and mechanochemical methods. Experimental data is shown in black while simulated data is shown in red.

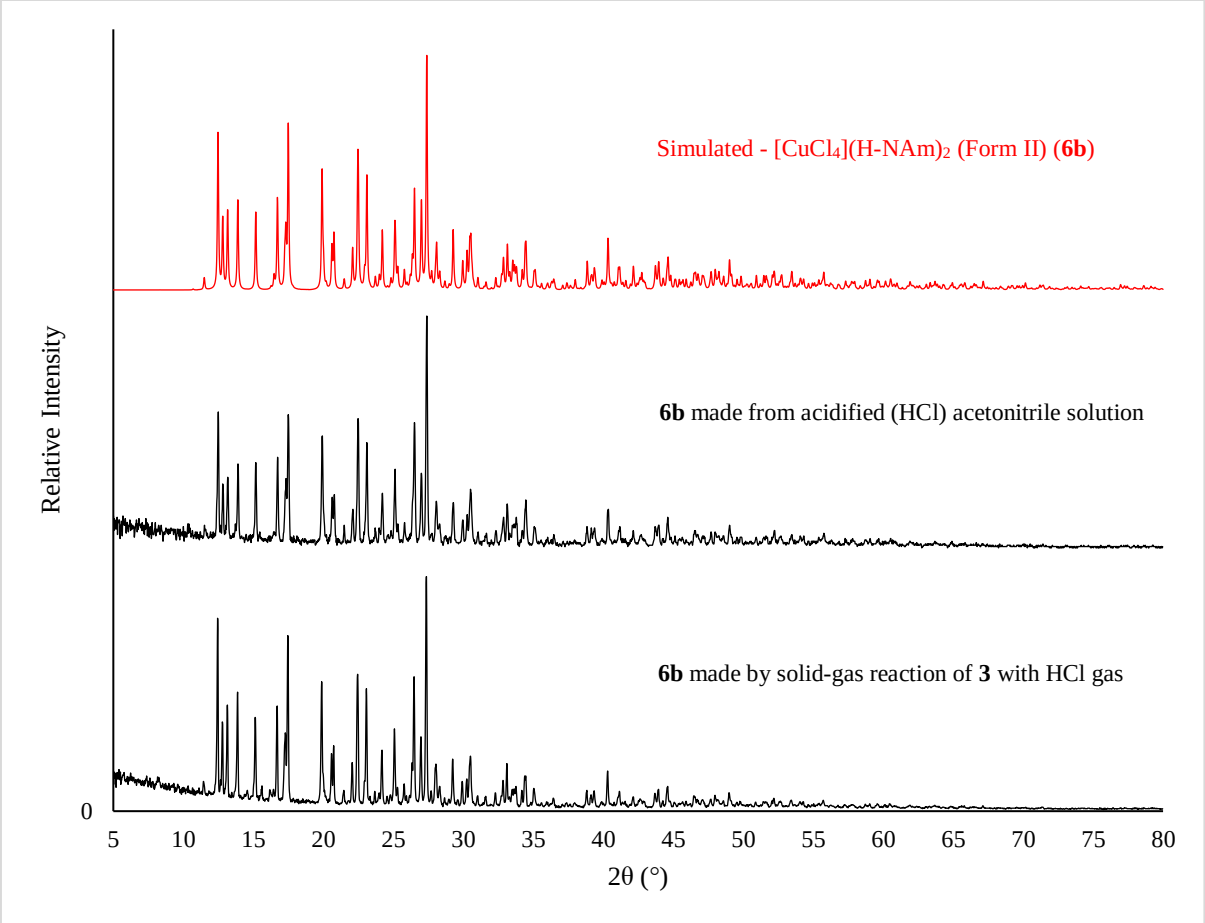

Figure S25. Room temperature X-ray powder diffraction data for samples of **6b** made from solution and solid-gas reaction of **3** with HCl gas. Experimental data is shown in black while simulated data is shown in red.

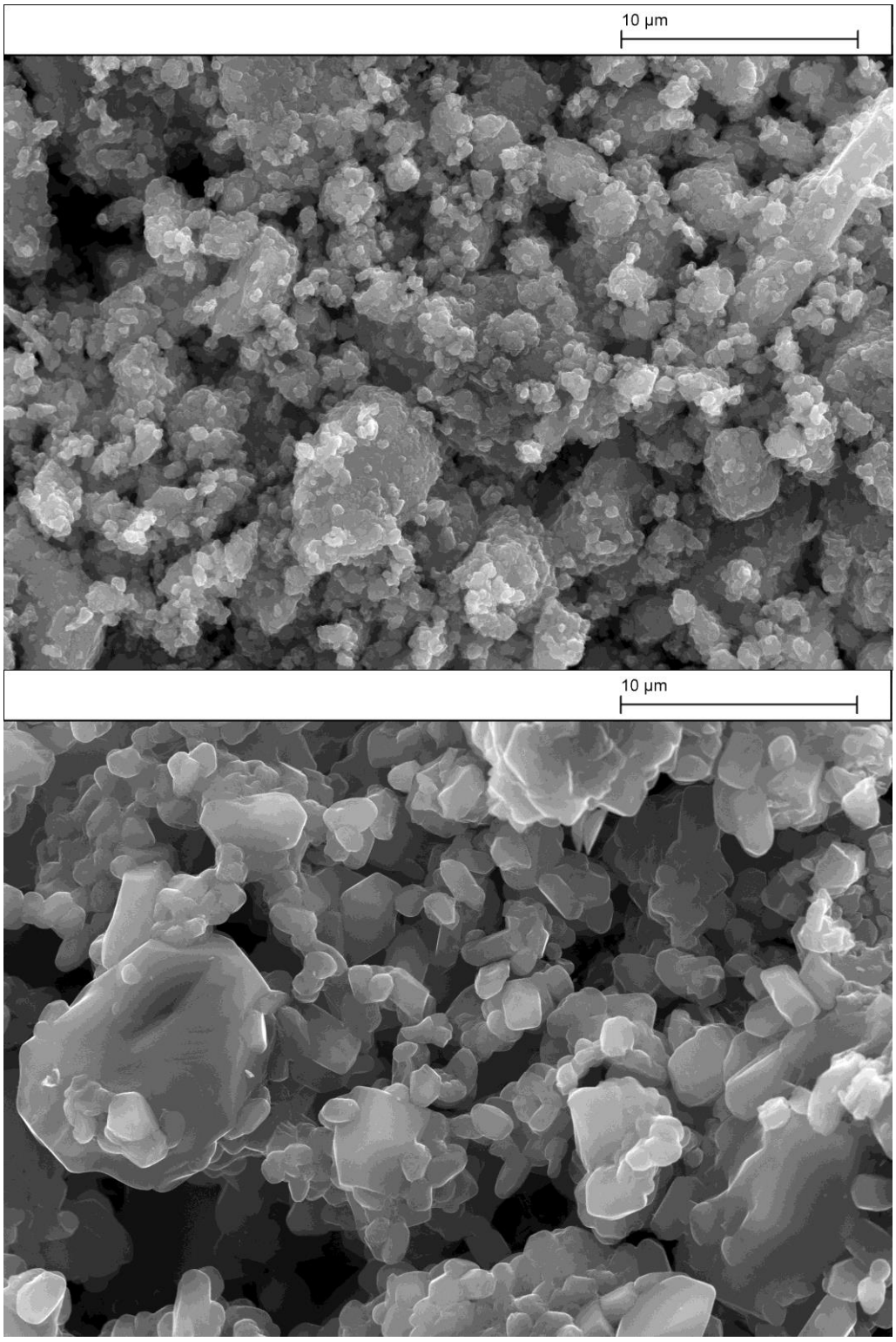

Figure S26. Scanning electron microscope images of $[CuCl_2(INAc)_2]_n$ (**1**) before (above) and after (below) exposure to HCl vapour, the latter producing a powder of $[CuCl_4](H\text{-}INAc)_2$ (**4b**).

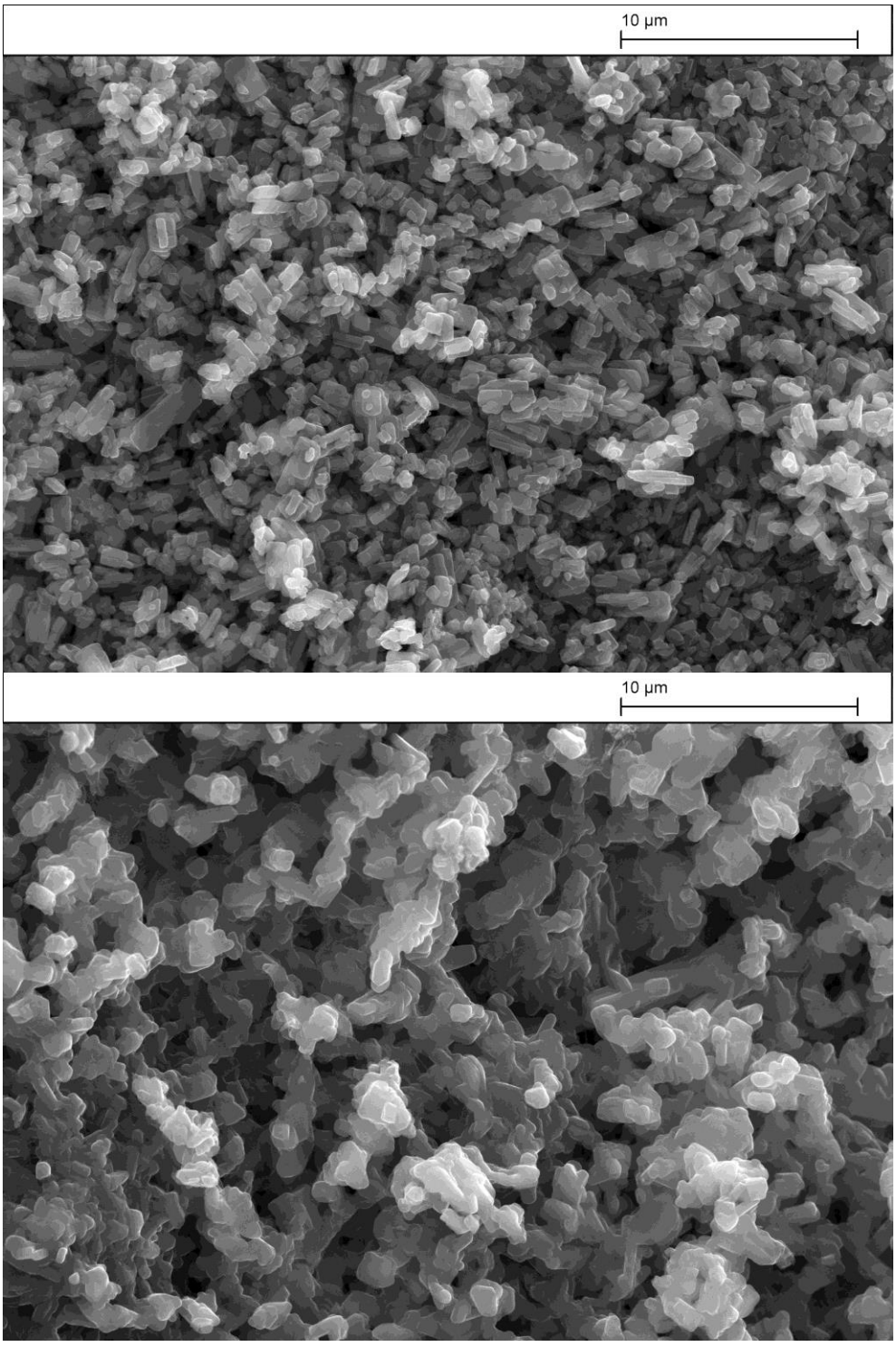

Figure S27. Scanning electron microscope images of $[CuCl_2(INAm)_2]_n$ (**2**) before (above) and after (below) exposure to HCl vapour, the latter producing a powder of $[CuCl_4](H\text{-}INAm)_2$ (Form II) (**5b**).

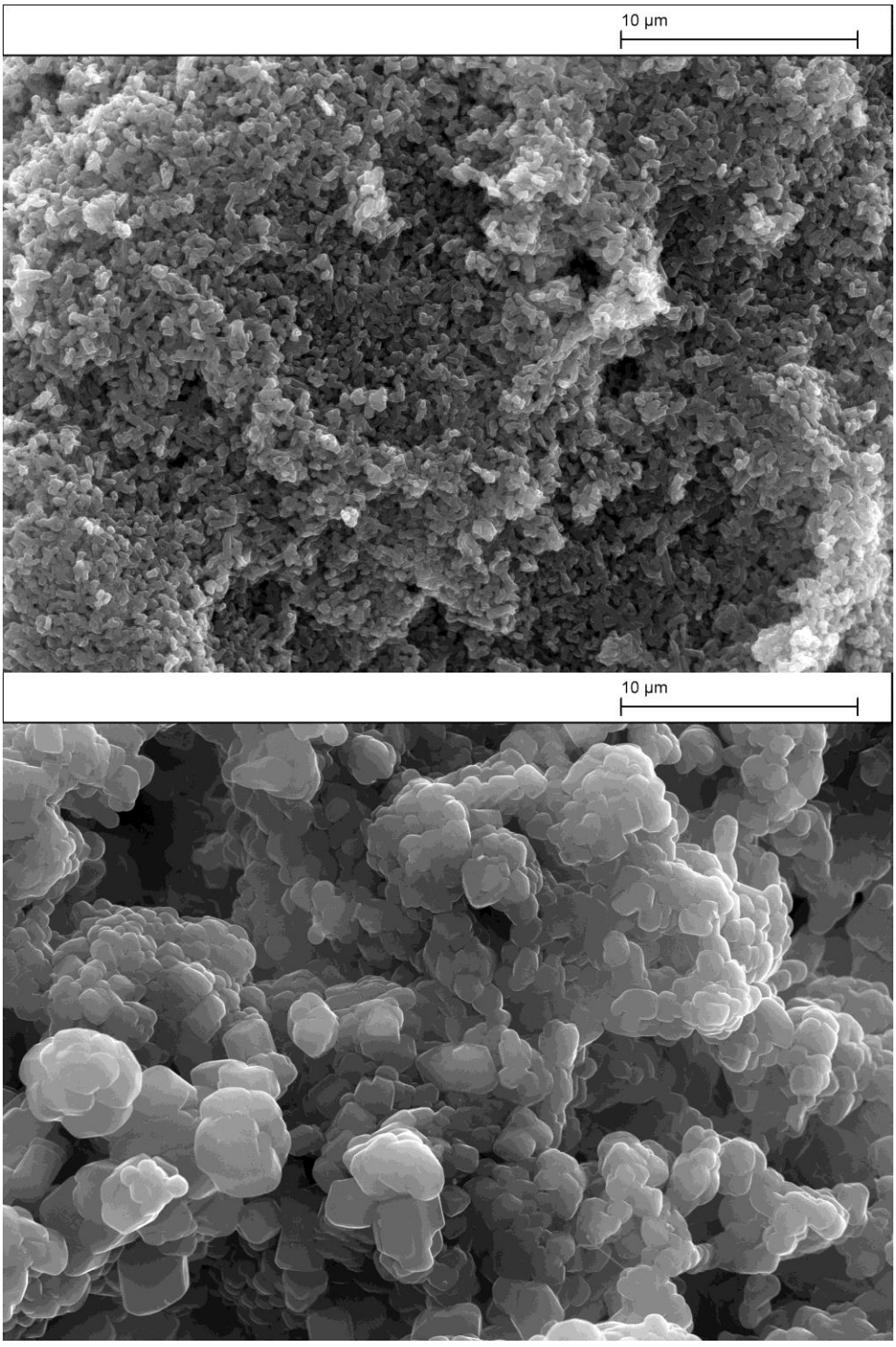

Figure S28. Scanning electron microscope images of $[CuCl_2(NAm)_2]_n$ (**3**) before (above) and after (below) exposure to HCl vapour, the latter producing a powder of $[CuCl_4](H\text{-}NAm)_2$ (Form II) (**6b**).